



A new shergottite martian meteorite analog system (SAS) for alteration experiments

V. Fortier^{a,b,*}, V. Debaille^b, V. Dehant^{a,c}, B. Bultel^d

^a Earth and Life Institute, Université Catholique de Louvain-la-Neuve, Louvain-la-Neuve, Belgium

^b Laboratoire G-Time, Université libre de Bruxelles, Bruxelles, Belgium

^c Royal Observatory of Belgium, Bruxelles, Belgium

^d Geosciences Paris Saclay, Université Paris-Saclay, Paris, France

ARTICLE INFO

Keywords:

Mars
Analog
Shergottite
Hydrothermalism
Serpentinization
Fischer-tropsch type (FTT) reactions

ABSTRACT

Martian rocky material available on Earth has been so far composed of meteorites and is limited in terms of mass and number. This restricted amount directly impairs the possibility to perform destructive analyses and experiments requiring large mass of sample, such as alteration and hydrothermal experiments. One of the main intents of the current Mars Sample Return (MSR) mission is to bring rock samples from Mars to Earth in the next 10 years. While we will have a geological context for the samples, the total mass that will be collected will also be limited. It is thus crucial to seek analogs of martian rocks, not suffering from this limitation while bearing specific martian properties required by the planned experiments.

To overcome this problem in the frame of alteration and hydrothermal experiments, we have built a flexible powder analog system to mimic a typical non-altered shergottite from a chemical and mineralogical perspective. To do so, we have selected the six main mineral phases in weight percentage present in shergottites. For each phase we selected multiple pure terrestrial mineral powders chosen for their chemistry close to their shergottite counterparts. As these mineral phases come from only three different relatively easy access locations, the assemblage is virtually unlimited.

From the Shergottite Analog System (SAS), the Shergottite Sample Powder (SSP)-1 analog has been created to focus on serpentinization and abiotic methane formation experiments under martian conditions. The SAS could also be used to create analogs of Oxia Planum, Gale Crater, or Jezero Crater, and to test possible detection interferences and to determine the sensitivity of multiple analytic techniques by varying the selected phases and their proportions.

1. Introduction

Until the future arrival on Earth of the first rocks directly sampled on Mars, the only ones available are the martian meteorites present on Earth. So far, more than 300 martian meteorites (Meteoritical Bulletin Database) have been identified that can be used for non-destructive, invasive, and destructive analyses, or even as calibration targets on board rovers working on Mars, usually using from a few milligrams (mg) to a few grams (g) of sample (Fries et al., 2022; Cousin et al., 2022). On the other hand, some types of experimental work, such as reproducing rock alteration under martian conditions, may require from tens to hundreds of grams of sample. The realization of experimental work could thus be potentially impaired due to the limited amount of material

available, and the destructive nature of those works.

To address this sample availability limitation, terrestrial analogs have been developed and used for many years to simulate martian material (Karl et al., 2022) such as regolith (Allen et al., 1998; Peters et al., 2008; Cannon et al., 2019; Ramkissoon et al., 2019) and rocks (Edwards et al., 1999; Wentworth et al., 2005; Bost et al., 2013; Bost et al., 2015; Cloutis et al., 2015; Manzari et al., 2016; Hickman-Lewis et al., 2020, Planetary and Terrestrial Analogs Library (PTAL): Dypvik et al., 2021, McKinney Basalt: Leeman and Vitaliano, 1976, Adcock et al., 2018, and the European Space Agency (ESA) Sample Analogue Curation Facility (SACF)). Usually, an analog will be developed for a specific purpose, for example to mimic mechanical properties of their martian counterparts for driving tests. For such case, its chemical

* Corresponding author. Earth and Life Institute, Université Catholique de Louvain-la-Neuve, Louvain-la-Neuve, Belgium.

E-mail address: valentin.fortier@uclouvain.be (V. Fortier).

<https://doi.org/10.1016/j.pss.2023.105749>

Received 14 April 2023; Received in revised form 26 June 2023; Accepted 21 July 2023

Available online 24 July 2023

0032-0633/© 2023 Elsevier Ltd. All rights reserved.

composition has not been targeted, and thus cannot be re-used as geochemical analog for studies aiming to investigate geochemical processes. On the other hand, finding a match between mineralogical and chemical characteristics of terrestrial and martian rocks is challenging as formation conditions are unique on each planetary body.

The detection of methane (CH₄) by the Curiosity rover (Webster et al., 2015) and its potential abiotic formation in past or present hydrothermal systems sustaining serpentinization (Oze and Sharma, 2005) has fueled the need to reproduce experimentally such hydrothermal systems under present martian conditions. The target for our analog system is the first ~ 3 – 20 kilometers (km) under the surface of Mars (depending on thermal gradient link to the period) where conditions for liquid water (H₂O) could be met. As such, we are aiming for the material that could be currently witnessing such hydrothermal systems, i.e. the more recent material that would represent the martian outermost kilometers. More specifically, we are targeting material composition and mineralogy, with a particular focus on the reactive species, i.e. the minerals involved in serpentinization and the metallic-rich phases able to act as catalyst for abiotic CH₄ formation by Fischer Tropsch Type reactions.

Numerous experimental works have been realized targeting serpentinization in Mars-like conditions (Berndt et al., 1996; Barbier et al., 2020 and references within, McCollom et al., 2022). However, it was often either mono-mineral, approximate chemical composition, or bulk terrestrial samples that were used in those experiments, missing either similarity with Mars or control over the sample chemistry and mineralogy. To try to overcome such problematics, we have developed an analog system based on the mix of different pure terrestrial minerals, thus characterized as a second-generation simulant system based on the terminology of Karl et al., (2022). For that, we selected pure individual minerals from specific locations on Earth for their compositions similar to their martian counterparts. The minerals can then be mixed at will in different proportions, allowing creation of numerous different analogs. As every analog (Foucher et al., 2021), we have developed our analog system in a specific frame and aimed to mimic at best the following characteristic: mineral proportion, mineral chemistry, and bulk chemistry.

2. Analog characteristics determination

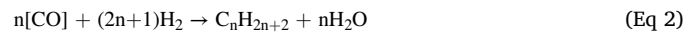
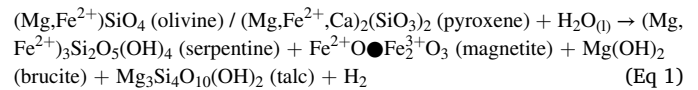
2.1. Experimental goal for SAS development

We have developed our analog system in the specific frame of alteration experiments, and more specifically targeting serpentinization reaction and the abiotic formation of methane by Fischer Tropsch Type reaction.

Serpentinization is a hydrothermal process where ferrous iron-bearing silicates, typically olivine and pyroxene from igneous mafic/ultra-mafic rocks are oxidized by liquid water, to form ferric iron and secondary minerals such as magnetite, brucite, talc, or serpentine (giving its name to the reaction) (Oze and Sharma, 2005) (Eq (1)). It also produces molecular dihydrogen by water reduction, potentially used as energy source by life, but also as reactant for Fischer Tropsch Type (FTT) reactions. Serpentinization reaction happens at a wide range of temperature from < 25 °C up to ~ 500 °C (Barnes et al., 1978; Allen and Seyfried, 2003; Okland et al., 2014), with optimal temperature around 280 °C for olivine and > 400 °C for pyroxene (Martin and Fyfe, 1970).

Serpentinization is known to have happened in the past of Mars during Noachian, where liquid water activity was strong. It is confirmed by orbital and in-situ detection of serpentine (Ehlmann et al., 2009, 2010; Michalski and Niles, 2010; Bultel et al., 2015; Viviano-Beck et al., 2017; Amador et al., 2017, 2018; Brown et al., 2023). On Earth, serpentinizing hydrothermal environments are often tied to local ecosystem (Bradley and Summons, 2010; McCollom and Seewald, 2013, Ménez, 2020) and to methane detection (Schrenk et al., 2013 and references within). This methane detection can be explained by local processes able to generate hydrocarbons, such as biotic ones with

methanogens microbes, or abiotic ones with the FTT reactions (McCullom and Seewald, 2007; Etiope and Sherwood Lollar, 2013; Schrenk et al., 2013 and references within).



Fischer Tropsch Type reactions are metal-catalyzed carbon hydrogenation abiotic processes forming methane and other hydrocarbons. Dihydrogen reacts with a carbon source (CO or CO₂) to form hydrocarbons in general (including methane in particular) and water (Eq (2)). Those reactions are efficient at high temperatures up to > 500 °C and have been successfully tested at temperatures as low as 20 °C (Etiope and Ionescu, 2015). They require metallic catalysts, with Fe, Ni, and Cr commonly considered to sustain the reactions. It is commonly the Sabatier CO₂ specific version (Eq (3)) of the FTT reactions which is considered on Earth due to the global low abundance of CO in natural system. Despite being quite sluggish and unlikely in saturated water environment (Miguel et al., 2015; Duyar, 2015), Sabatier reaction can take place in serpentinization hydrothermal system where local gas phase is present, hence allowing direct gas-rock interactions and production of H₂ (McCullom, 2016). Both the H₂ and CH₄ formed can be a potential energy source for microorganisms, such as methanotrophs, to sustain local ecosystems.

Due to their potential link to life on Earth and on other planetary bodies, those reactions have been thoroughly studied experimentally under Earth and Mars hydrothermal conditions (Barbier et al., 2020 and references within, McCollom et al., 2022). Bulk rock or minerals are commonly used crushed in those experiments to increase the reaction surfaces and to kinetically speed up the reactions, with particle size varying from 1 to a few hundreds micrometers (µm) (Barbier et al., 2020 and references within, McCollom et al., 2022).

2.2. SAS target and characteristics

The objective of our analog system is to reproduce at best the petrological and chemical characteristics of the most recent pristine magmatic material available on Mars. While it is now acknowledged that martian meteorites are not fully representative of the martian crust (McSween, 2015; Bouvier et al., 2018), the current remote sensing data do not allow a very fine characterization of mineral species, especially the ones in small quantities, even though some might be important in term of reactivity. As such, we decided to start our analog from the best characterized material from Mars available on Earth: the martian meteorites.

Among martian meteorites, we have selected shergottite finds from Antarctica and the shergottite falls Shergotty, Zagami, and Tissint. Antarctica has low temperature, low humidity, and biological activity is almost non-existent on the surface, allowing good preservation of the meteorites through time compared to finds from hot deserts (Croaz and Wadhwa, 2001; Croaz et al., 2003; Pourkhorsandi et al., 2021; Maeda et al., 2021). Falls were considered also for their lack of terrestrial contamination and alteration. Only shergottites were considered among the martian meteorites family for this analog system for the following reasons:

- 1) Shergottites represent 84 % of the total martian collection by number, and also by mass. They are basaltic rocks, thus with an igneous mineralogy based on pyroxene and plagioclase, and with a significant content in olivine. The proportion of the different mineral phases vary significantly from one shergottite to another. They are classified chemically by their relative concentrations in Incompatible

Table 1
Antarctica shergottites mineral proportions (vol%).

Phase	Mineralogy (vol%)								TOTAL
	Name	Olivine	Augite	Pigeonite	Opx	Chromite	Maskelynite	Other	
Shergotty	<i>n.d.</i>	34.6	34.6	<i>n.d.</i>	<i>n.d.</i>	22.9	6.8	99.8	
Zagami	<i>n.d.</i>	37.9	37.9	<i>n.d.</i>	<i>n.d.</i>	18.1	6.0	99.8	
Tissint	26.5		51.0		<i>n.d.</i>	21.0	1.5	100.0	
EETA 79001 A	8.9	6.1	59.3	5.4	<i>n.d.</i>	17.1	3.3	100.1	
EETA 79001 B	<i>n.d.</i>	19.9	39.5	<i>n.d.</i>	<i>n.d.</i>	29.1	4.6	93.1	
QUE 94201	5.6		48.8	0.1		43.1	2.3	99.9	
ALH 77005 Y 1075	44.2	11.0	26.0	9.5	1.5	9.9	1.2	103.3	
LEW 88516	45.9		11.9	25.1	0.8	7.0	9.1	99.8	
Y 793605	40.0	17.0		33.0	1.0	8.0	1.0	100.0	
Y 980459 Y 980497	15.7		24.7	27.9	0.5	<i>n.d.</i>	32.1	100.9	
Y 000027 Y 000047 Y 000097 Y 984028	40.0	9.7		39.3	1.4	8.6	1.0	100.0	
GRV 99027	32.1	5.0	<i>n.d.</i>	55.4	1.1	5.8	0.7	100.1	
Y 002712 Y 002192	<i>n.d.</i>	43.0	27.0	<i>n.d.</i>	<i>n.d.</i>	29.0	<i>n.d.</i>	99.0	
GRV 020090	28.3	11.5	38.7	<i>n.d.</i>	1.4	18.9	1.1	99.9	
RBT 04261 RBT 04262	40.8	11.6	24.8	<i>n.d.</i>	1.6	18.1	1.7	98.6	
LAR 12095 LAR 12240	16.5		60.5		<i>n.d.</i>	22.0	1.0	100.0	
LAR 06319 LAR 12011	24.4	22.2	27.7	4.1	<i>n.d.</i>	17.8	3.7	99.9	
MEAN	20.6	18.1	29.9	10.1	0.5	16.5	4.3	100.0	
Min	0.0	5.0	0.0	0.0	0.0	0.0	0.0	/	
Max	45.9	43.0	59.3	55.4	1.6	43.1	32.1	/	

Meteorites are grouped by suggested pairing based on The Martian Meteorite Compendium. The mean values of the same pairing meteorites are used. When one of the paired meteorites is better characterized (black) than the others (grey), we use this specific meteorite values instead of a mean. Mean, minimum, and maximum values are recalculated at 100 vol%. "n.d." for Not Determined. Data gathered from The Martian Meteorite Compendium and references within (Burghelle et al., 1983; Hamilton et al., 2003; Balta et al., 2015; Lodders, 1998, Lin et al., 2005).

Table 2
Mean (min-max) oxide composition (wt%) of the six mineral phases in the considered shergottites.

	Olivine	Pigeonite	Augite	Orthopyroxene	Maskelynite	Chromite
<i>End members</i>	<i>Fe_{67.7}</i> (58.4-79.2)	<i>En_{60.3}</i> (35.5-70.6) <i>Fs_{30.8}</i> (22.9-53.4)	<i>En_{45.1}</i> (29.5-50.5) <i>Fs_{21.3}</i> (13.6-46.3)	<i>En_{69.9}</i> (65.6-73.1) <i>Fs_{23.8}</i> (21.7-24.9)	<i>An_{49.9}</i> (39.1-59.7) <i>Ab_{47.9}</i> (40.0-54.8)	<i>Cr_{#36.0}</i> (29.9-39.8) <i>Al_{#9.5}</i> (6.5-19.3)
Al ₂ O ₃ (wt%)	0.06 (0.02-0.15)	0.78 (0.64-0.87)	1.65 (0.89-2.03)	0.62 (0.36-0.99)	27.00 (25.42-28.30)	8.57 (5.88-16.40)
CaO	0.17 (0.01-0.23)	4.40 (3.26-5.63)	16.17 (11.05-18.08)	2.97 (1.43-4.77)	9.98 (8.03-11.51)	0.08 (0.00-0.20)
Cr ₂ O ₃	0.10 (0.02-0.41)	0.38 (0.10-0.61)	0.66 (0.03-0.88)	0.43 (0.40-0.50)	0.01 (0.00-0.04)	46.85 (39.12-51.30)
FeO _(t)	27.89 (19.01-35.09)	18.85 (14.73-31.20)	12.89 (8.22-27.22)	14.87 (13.13-16.12)	0.64 (0.36-1.44)	34.27 (29.85-41.12)
K ₂ O	0.01 (0.00-0.02)	0.01 (0.00-0.02)	0.01 (0.00-0.02)	0.00 (0.00-0.00)	0.36 (0.04-0.95)	0.01 (0.00-0.01)
MgO	33.49 (28.04-40.52)	21.18 (11.60-25.82)	15.40 (9.71-17.87)	25.91 (23.38-18.65)	0.16 (0.07-0.28)	4.47 (3.02-5.82)
MnO	0.55 (0.43-0.65)	0.60 (0.49-0.81)	0.46 (0.37-0.76)	0.51 (0.42-0.60)	0.02 (0.00-0.04)	0.50 (0.41-0.60)
Na ₂ O	0.02 (0.00-0.04)	0.07 (0.03-0.10)	0.21 (0.12-0.27)	0.06 (0.02-0.10)	5.33 (4.26-6.20)	0.01 (0.00-0.02)
NiO	0.10 (0.06-0.018)	0.05 (0.03-0.07)	0.08 (0.03-0.10)	<i>n.d.</i>	0.01 (0.00-0.03)	0.10 (0.10-0.10)
P ₂ O ₅	0.20 (0.01-0.50)	0.12 (0.01-0.24)	0.11 (0.02-0.16)	0.00 (0.00-0.00)	0.05 (0.00-0.13)	0.08 (0.05-0.10)
SiO ₂	37.38 (35.53-39.55)	53.21 (49.20-54.51)	51.82 (48.31-53.09)	54.42 (53.02-55.21)	56.34 (54.13-58.33)	0.19 (0.01-0.66)
TiO ₂	0.03 (0.01-0.06)	0.35 (0.12-0.81)	0.55 (0.30-0.80)	0.20 (0.08-0.50)	0.09 (0.00-0.17)	4.87 (3.36-6.92)

Total wt% of each mineral phase has been recalculated at 100 wt%."n.d." for Not Determined.

Trace Elements (ITE), and by petrology based on their texture and mineralogy (Udry et al., 2020). Their ITE define three distinct groups being the depleted, the intermediate, and the enriched shergottites. Their mineralogy and texture define six distinct groups: (1) Poikilitic, with olivine enclosed in large pyroxene crystals. (2) Brecciated, (3) Diabasic, microgabbroic. (4) Gabbroic. (5) Olivine-phyrlic, with high proportions of olivine phenocrysts. (6) Fine-grained shergottites. Ejection ages indicate that shergottites are likely coming from a limited number of ejection events (Lapen et al., 2017; Wieler et al., 2016; Udry et al., 2020). The depleted shergottites seem to have been ejected in one unique event at 1.1 ± 0.4 million years (Myr) ago (Lapen et al., 2017), and the other shergottites have ejection ages varying from ~ 2 to 5 Myr (Wieler et al., 2016). This limited amount of ejection events indicates that shergottites represent a few locations on Mars, hence questioning their representativity at a planetary scale. However, the available samples, either for mineralogy of chemical composition, indicate a diverse chemistry and mineralogy. As such, shergottites provide a solid and diverse database to represent at least partially the most recent magmatism on Mars.

2) Shergottite crystallization ages have been determined using radiogenic isotope systems such as ^{87}Rb - ^{87}Sr , ^{147}Sm - ^{143}Nd , ^{176}Lu - ^{176}Hf ,

and U-Pb. The crystallization ages vary from 147 Myr for Shergotty, around 200 Myr for enriched and intermediate shergottites, to finally less than 500 Myr for depleted shergottites (Nyquist et al., 2001; Udry et al., 2020). Two peculiar shergottites NWA 7635 and NWA 8159 are both dated at ~ 2.4 billion years (Gy) (Udry et al., 2020). Those relatively young ages indicate that they reasonably record young magmatic events at the surface of Mars that could have provided heat to sustain recent hydrothermal activity as would be required for present-day methane observations (Webster et al., 2015).

3) It has been suggested that andesitic magmatism could have existed very early in Mars history based on zircon study (Bouvier et al., 2018), magma ocean crystallization models (Elkins-Tanton, 2008; Elkins-Tanton et al., 2005), and in-situ observations of rocks with evolved composition (Sautter et al., 2015). In addition, recent seismic data from the Insight lander proposed a crust density inferior to basaltic one, thus leaning toward a more felsic composition (Wieczorek et al., 2022). However, a basaltic composition is nonetheless proposed as representative of the bulk martian crust based on available geochemical data (McSween, 2015; McSween et al., 2009). The shergottite nature indeed matches a basaltic crust.

Table 3
Chemical composition (wt%), endmembers, and available weight of the mineral phases used in the analog system.

Phase	High-Calcium Clinopyroxene ^a										Orthopyroxene ^b				Plagioclase ^a				Chromite									
	Olivine ^a	9-1920.5		9-2111.5		9-2236		9-1302.5		9-1473.5		9-1920.5		9-2111.5		00-63		00-65		00-70		9-468		9-514		9-538		
Sample Weight (g)		59.93	9-1473.5	9-1920.5	9-2111.5	9-2236	9-1302.5	9-1473.5	9-1920.5	9-2111.5	00-63	00-65	00-70	9-468	9-514	9-538												
End members		Fo _{66.9}	Fo _{66.9}	Fo _{66.0}	Fo _{66.9}	Fo _{66.9}	Fo _{66.9}	Fo _{66.9}	Fo _{66.9}	Fo _{66.9}	Fo _{66.9}	Fo _{66.9}	Fo _{66.9}	Fo _{66.9}	Fo _{66.9}	Fo _{66.9}												
Al ₂ O ₃		0.02	0.02	0.03	0.03	0.03	0.03	0.03	0.03	0.03	0.03	0.03	0.03	0.03	0.03	0.03												
CaO		0.07	0.05	0.05	0.05	0.05	0.05	0.05	0.05	0.05	0.05	0.05	0.05	0.05	0.05	0.05												
Cr ₂ O ₃		/	/	/	/	/	/	/	/	/	/	/	/	/	/	/												
FeO ₍₀₎		29.01	29.25	29.77	29.16	29.16	29.16	29.16	29.16	29.16	29.16	29.16	29.16	29.16	29.16	29.16												
K ₂ O		0.00	0.01	0.02	0.01	0.01	0.01	0.01	0.01	0.01	0.01	0.01	0.01	0.01	0.01	0.01												
MgO		32.93	32.80	32.36	33.03	33.03	33.03	33.03	33.03	33.03	33.03	33.03	33.03	33.03	33.03	33.03												
MnO		0.43	0.45	0.43	0.44	0.44	0.44	0.44	0.44	0.44	0.44	0.44	0.44	0.44	0.44	0.44												
Na ₂ O		0.01	0.00	0.02	0.02	0.02	0.02	0.02	0.02	0.02	0.02	0.02	0.02	0.02	0.02	0.02												
NiO		/	/	/	/	/	/	/	/	/	/	/	/	/	/	/												
P ₂ O ₅		/	/	/	/	/	/	/	/	/	/	/	/	/	/	/												
SiO ₂		37.41	37.26	36.96	37.60	37.60	37.60	37.60	37.60	37.60	37.60	37.60	37.60	37.60	37.60	37.60												
TiO ₂		0.03	0.02	0.02	0.02	0.02	0.02	0.02	0.02	0.02	0.02	0.02	0.02	0.02	0.02	0.02												
TOTAL		99.91	99.86	99.66	100.36	100.36	100.15	100.15	100.15	100.15	100.15	100.15	100.15	100.15	100.15	100.15												

^a Data from Namur et al., (2010).
^b Data from Charlier et al., (2005).

Regarding nakhlites and chassignites, they represent ~ 10 % of the martian meteorite collection, and are likely to have originated from one short interval of magmatism around 1.34 Gyr ago (Udry and Day, 2018), displaying a very limited range of mineralogical composition. Moreover, nakhlites and chassignites were ejected from Mars by a unique ejection event dated at ~ 11 Myr, thus representing only one specific location on Mars (Treiman, 2005; Nyquist et al., 2001). This old crystallization age and their mono-origin on the martian surface preclude their use for hydrothermal experiments in young martian basalts.

Among martian ungrouped meteorites, NWA 7533/7034 analyses indicated that it provides the best match with orbiters and rovers data (Agee et al., 2013; Humayun et al., 2013). However, it is a breccia composed of many different small clasts, making it quite complex to reproduce as an analog. Thus we have not considered it.

Thirteen well-characterized Antarctic shergottite meteorites/paired meteorites were selected, in addition to the Shergotty, Zagami, and Tissint shergottites falls (Table 1). Among the Antarctic ones, seven are poikilitic (ALH 77005, LEW 88516, Y 793605, Y 000097, GRV 99027, GRV 020090, RBT 04261/04262), four are olivine-phyric (EETA 79001 A, Y 980459, LAR 12095/12240, LAR 06319/12011), two are diabasic (QUE 94201, Y 002712), and one is fine grained (EETA 79001 B). Regarding their ITE content, three are depleted (LAR 12095/12240, Y 980459, QUE 94201), eight are intermediate (ALH 77005, GRV 020090, GRV 99027, LEW 88516, Y 000097, Y 793605, EETA 79001 A, EETA 79001 B), and two are enriched (RBT 04261/04262, LAR 06319/12011). Shergotty, Zagami, and Tissint are respectively an enriched diabasic, an enriched fine-grained, and an olivine-phyric fall shergottites. The three ITE based groups, and four of the six petrological groups of shergottites are represented, showing a robust representation of shergottite in general.

To limit the complexity of the Shergottite Analog System (SAS), the first six more abundant and reactive mineral phases identified from the considered meteorites are examined: olivine, high-calcium clinopyroxene (augite), low-calcium clinopyroxene (pigeonite), orthopyroxene, plagioclase (maskelynite), and chromite. Olivine and pyroxene are reactants during the serpentinization and contain Fe, in addition to trace amount of Ni and Cr respectively, all three potential catalysts for FTT reactions. Chromite is made of Fe and Cr, again potential catalysts for FTT reactions (Foustoukos and Seyfried, 2004; Horita and Berndt, 1999). We exclude other minor phases such as spinel (other than chromite), phosphates, sulfides, oxides, and glass due to (1) their low relative proportion < 4 volume percentage (vol%) on average (see Table .1), and even absence in some of the considered meteorites; (2) their chemical variability; (3) their potential secondary origin (alteration or impact); and (4) their potential effect as poorly constrained FTT catalysts thus obscuring olivine, pyroxene, and chromite effects. Those minor phases would need to be considered in the future, but this is a whole complex research topic and beyond the scope of the paper.

Proportions and chemistry of each of those phases are determined from previous studies done on martian meteorites (Martian Meteorite Compendium, McSween and Jarosewich, 1983, Lodders, 1998, Ma et al., 1981, Treiman, 1994, Mikouchi and Miyamoto, 1997, Greshake et al., 2004, Mikouchi and Kurihara, 2008, Lin et al., 2005, Jiang and Hsu, 2012, Usui et al., 2010, Dunham et al., 2019, Basu Sarbadhikari et al., 2009) and are presented in Table 1 and Table 2 respectively.

3. Mineral selection and preparation

From the six mineral phases targeted, isolated samples have been found for five of them: olivine (ol), high-calcium clinopyroxene (high-Ca cpx), orthopyroxene (opx), plagioclase (pl), and chromite.

Sample for low-calcium clinopyroxene (low-Ca cpx) could not been found due to its specific chemistry and the fact that pigeonite is often intergrown with augite without any clear contact (Müller, 1993). While we considered using a mixed pigeonite/augite natural assemblage instead of individual pigeonite and augite, it would have been

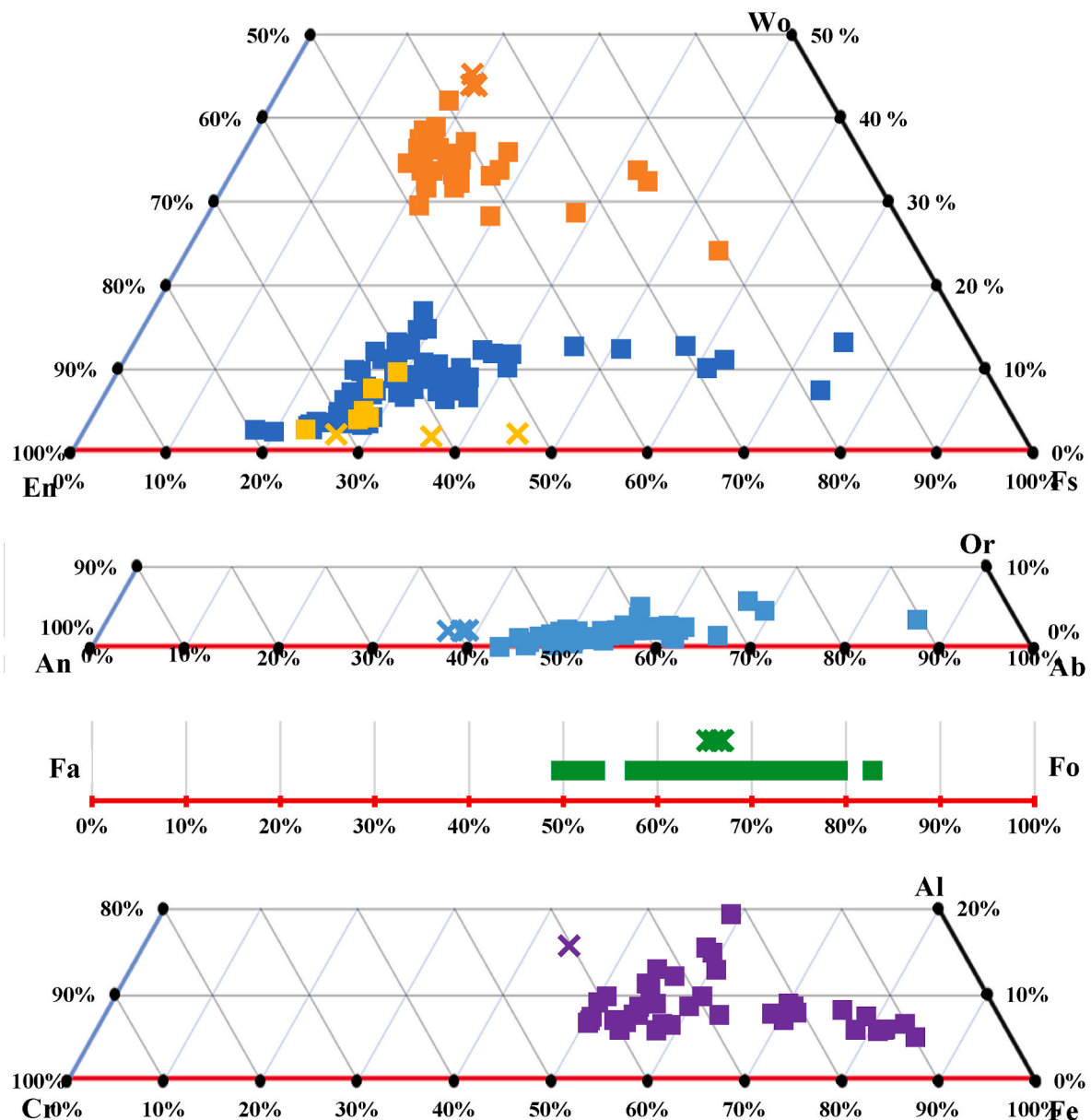


Fig. 1. Endmember comparison between our pure mineral phases (crosses) and considered shergottites (squares) for (top to bottom) high-Ca cpx (orange), low-Ca cpx (dark blue), opx (yellow), plagioclase (light blue), olivine (green), and chromite (purple). Data gathered from The Martian Meteorite Compendium and references within (Balta et al., 2015; Steele and Smith, 1982; Papike et al., 2009, Treiman, 1994, Gleason et al., 1997; Harvey et al., 1993; Hsu et al., 2004; Lin et al., 2005; Jiang and Hsu, 2012; Usui et al., 2010; Basu Sarbadhikari et al., 2009; Stöfler et al., 1986).

impossible to vary the pigeonite/augite proportion and chemistry beyond the one forced by the natural assemblage, hence lowering the flexibility of our SAS and forcing it into a terrestrial-like assemblage far from a martian-like one. As such, low-Ca cpx are presently not available for SAS. We acknowledge the lack of low-Ca cpx could have a direct impact on the alteration processes we wish to reproduce with our analog system, because pyroxene is a reactant of serpentinization, and its Fe and Cr content could play a role in FTT catalysis. We hope to be able to improve our analog in the future by considering low-Ca cpx.

The five olivines (9–1920.5, 9–2111.5, 9–2236, 9–1302.5, 9–1473.5), five high-calcium clinopyroxenes (9–1920.5, 9–2111.5, 9–1302.5, 9–1473.5), and the three plagioclases (9–468, 9–514, 9–538) come from a drill in the Sept Iles ferrobaltic layered intrusion in Canada (Namur et al., 2010), the three orthopyroxenes (00–63, 00–65, 00–70) from the Bjerkreim-Sokndal in Norway (Charlier et al., 2005), and the chromite from the Troodos ophiolite system in Cyprus (collected on the field). It is important to note that these phases have been selected

primarily for their chemistry, but also for their documentation, their available quantity, and their resampling possibility.

Major elements composition of each mineral was determined by ICP-OES in previously cited studies and are summarized in Table 3 with their endmembers, and the weight available for each sample. Endmembers are compared to the considered shergottites ones in Fig. 1. All our olivines and the orthopyroxene “00–65” perfectly match their shergottite counterparts. The other orthopyroxenes are broadly fitting as they are slightly Mg-poor compared to shergottites (En_{59-67} vs $\sim En_{66-77}$). High-Ca cpx are also broadly fitting, with a slightly higher Ca content ($\sim Wo_{45}$) compared to shergottites (Wo_{24-42}). Plagioclases ($\sim An_{64}$) nearly overlap shergottite ones (An_{36-62}). Finally, chromite has a lower Fe# of 37 compared to shergottite Fe#₄₃₋₇₅. While not perfect, the broad agreement between our minerals and their shergottite counterparts is sufficient for the purpose of the serpentinization experiments. Importantly, those minerals correspond also to the following criteria: being relatively pure, well characterized, available in sufficient quantity, and

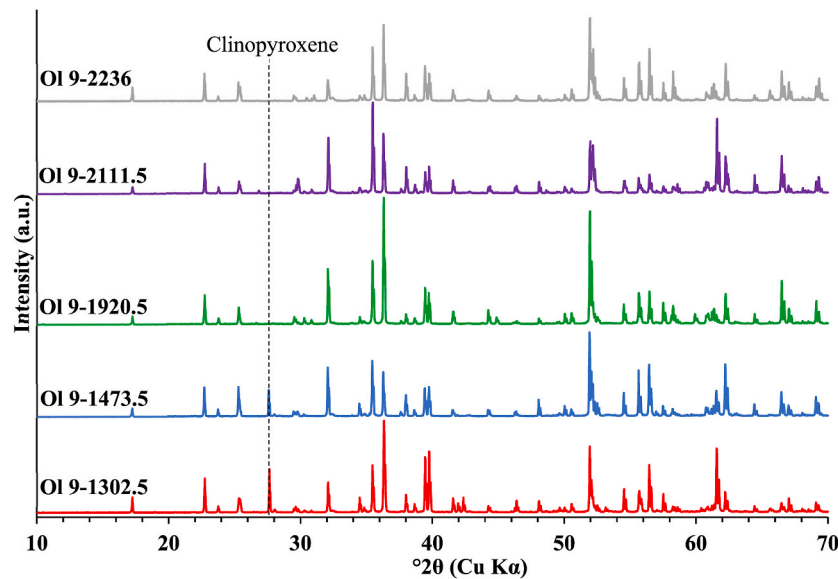


Fig. 2. XRD spectra of olivine 9–1302.5 (red), –1473.5 (blue), –1920.5 (green), –2111.5 (purple), –2236 (light grey) obtained using a Cu K α radiation source. Abscissa is in $^{\circ}2\theta$. Main peak for clinopyroxene is indicated as the dotted grey line.

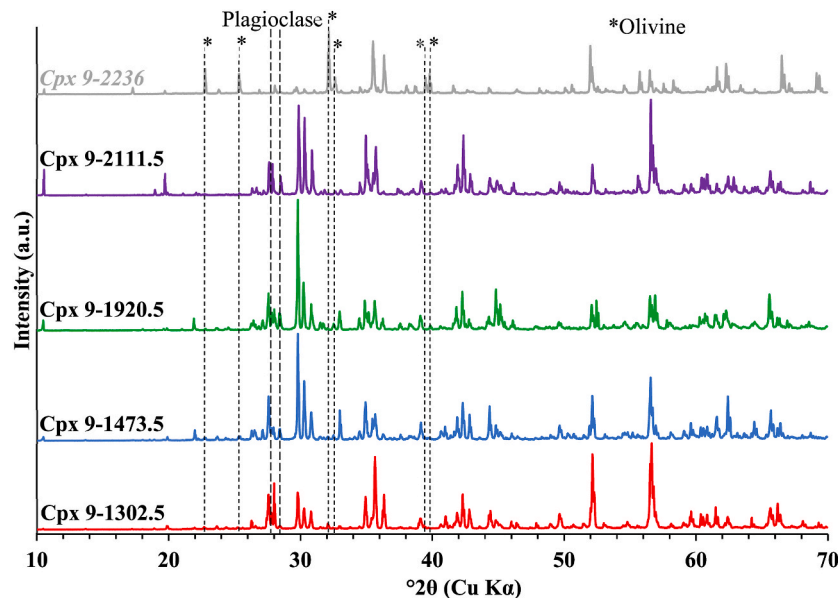


Fig. 3. XRD spectra of clinopyroxene 9–1302.5 (red), –1473.5 (blue), –1920.5 (green), –2111.5 (purple), –2236 (light grey) obtained using a Cu K α radiation source. Abscissa is in $^{\circ}2\theta$. Main peaks for olivine are indicated as the six dotted grey line and corresponding asterisks. Main peaks for plagioclase are indicated as the two dashed lines.

with a possibility to be resampled.

The different phases are kept as 75 – 250 μm powders. Olivines, high-Ca cpx, and opx were separated in previous studies by using heavy liquids (Namur et al., 2010; Charlier et al., 2005) and using an Isodynamic Frantz magnetic separator (Charlier et al., 2005). For olivines and high-Ca cpx, magnetic separation using an Isodynamic Frantz magnetic separator has been re-done for this study at the Laboratoire G-Time and was divided in two steps: a first step at 0.10 amp/ 15° tilt/ 15° slope to remove highly magnetic minerals such as magnetite and ilmenite, and a second step at 1.00 amp/ 15° tilt/ 15° slope to remove slightly magnetic minerals such as apatite, and separate olivine from high-Ca cpx. Remaining pyroxenes in the olivine fraction were removed by hand-picking, but only right before the use of the olivine to make an analog. Otherwise, they are kept with the olivine fraction.

Plagioclases have also been separated also by heavy liquids (Namur

et al., 2010).

Chromite is kept as a whole rock to avoid iron oxidation between use. When needed, the chromite was separated at the Laboratoire G-Time with an Isodynamic Frantz magnetic separator at 0.50 amp/ 15° tilt/ 15° slope to remove a slightly magnetic fraction likely to be non-chromitic material.

After separation, X-Ray Diffraction (XRD) analyses were done to check purity of each mineral. Those analyses were realized using a D8 Advance Eco Bruker diffractometer with a copper (Cu) anode Cu K α 1.5406 \AA , and using the Diffrac Suit software with the internal software and PDF-2 databases as references. Analyses were done at the 4MAT laboratory in Université Libre de Bruxelles (ULB), Belgium.

Less than 5 % of high-Ca cpx were detected in the olivine fraction (Fig. 2). Less than ~ 6 % of olivine and ~ 8 % feldspar were detected in the high-Ca cpx (Fig. 3). The high-Ca cpx 9–2236 was too contaminated

with olivine, and therefore we did not consider it to be a proper phase to include in our SAS. Those mineral mixtures are consistent with what is indicated in samples studies (Namur et al., 2010; Charlier et al., 2005). No contaminating phases were detected in the orthopyroxene or in the plagioclase fractions.

Each pure mineral phase is stored hermetically and individually after separation and purification. This individual storage allows us to have a flexibility in our SAS since we can create a wide range of different analogs by mixing specific phases and changing mineral proportion.

4. Analog uses

As stated previously, our flexible analog system has been developed in the objective to be used for alteration experiments in martian conditions, and more precisely on serpentinization and Fischer Tropsch Type (FTT) reactions. In this frame, from the SAS, we created a specific analog named Shergottite Powder Sample (SSP)-1, composed of olivine 9–1473.5 at 58.7 wt%, orthopyroxene 00–63 at 35.5 wt%, and chromite at 5.8 wt% that we are currently using for serpentinization and FTT experiments under martian conditions.

In addition to its main goal, SAS has also been proposed to the European Space Agency (ESA) in the frame of the ExoMars mission (postponed to 2028 at the present time) preparation as analog for the landing site of Oxia Planum on Mars. In Oxia Planum, analogs could be created to correspond to the capping unit known as the mantling unit, or to the base unit (Quantin-Nataf et al., 2021, Mandon et al., 2021) due to their basaltic composition with olivine and pyroxene detection.

Jezero Crater, the Mars2020 Perseverance rover landing site, has some geological units known to bear low-calcium and high-calcium pyroxene, plagioclases, and olivine (Mustard et al. 2007, 2009) that can also be mimicked by our analog system. More precisely, that is the case for the pyroxenes and olivines observed in the Séitah unit with compositions such as $Wo_{3-10}En_{44-50}Fs_{40-51}$ for low-Ca pyroxene, $Wo_{32-38}En_{38-44}Fs_{18-27}$ for high-Ca pyroxene, and Fo_{54-71} for olivine (Wiens et al., 2022) that globally overlap with the range of our analog system.

The Curiosity rover landing site of Gale crater has also units that could be globally mimicked by our mineral phases (Buz et al., 2017; Ehlmann and Buz. 2014), such as the Rocknest unit with its $\sim Fo_{62}$ olivine, $\sim An_{57}$ plagioclase, and $\sim En_{44}Fs_{18}Wo_{38}$ high-Ca clinopyroxene (Bish et al., 2013). The SAS can also be used to study possible detection interferences and to determine the sensitivity of multiple analytical techniques by varying the selected phases choice and their proportions. Those examples illustrate the adequacy of our SAS and its flexibility.

5. Conclusion and perspectives

We have developed an analog system to mimic at best the specific mineralogy of shergottites in the frame of alteration experiments in martian conditions, and more particularly for serpentinization hydrothermalism and abiotic methane (CH_4) production by Fischer Tropsch Type (FTT) reactions. This analog system was named SAS, standing for Synthetic Analog System, and makes available 16 different purified terrestrial mineral powders: five olivines, four high-Ca clinopyroxenes, three orthopyroxenes, three plagioclases, and one chromite, that are kept individually and can be mixed upon request. Those multiple powders allow a large variety of chemical compositions, implying high flexibility for the analog that can be created based on the SAS. It is a major improvement compared to mono-mineral or bulk terrestrial samples commonly used for igneous material analog.

In its current state, the SAS, is a promising modular tool for alteration and hydrothermal experiments in present martian-like conditions. Moreover, it can also be used to mimic specific martian igneous terrains such as Gale Crater, Jezero Crater, or Oxia Planum; thus helping in-situ data interpretation or preparation of future in-situ missions. The SAS

will still be in use after the return of martian samples after 2031 (Muirhead et al., 2020). Indeed, while precise measurements of those samples will refine the analog, the amount brought back to Earth will still not be sufficient for most experimental work.

Currently, one of the drawbacks is the absence of suitable low-Ca cpx that could not be found so far. Also, our current high-Ca cpx have a limited overlap with what we are aiming as martian composition range. This can be explained by the fact that low-Ca cpx and high-Ca cpx are often found tangled together without properly delimited contact, adding another difficulty for the mineral selection and separation. The SAS is intended to evolve and be improved to match at best our current target rocks, and to match a wider spectrum of martian compositions.

Declaration of competing interest

The authors declare that they have no known competing financial interests or personal relationships that could have appeared to influence the work reported in this paper.

Data availability

Data will be made available on request.

Acknowledgments

Valentin Fortier, Vinciane Debaille, and Véronique Dehant would like to thank the EOS (Excellence Of Science) ET-Home (Evolution and Tracers of the Habitability Of Mars and Earth) project funded by the FNRS (Fonds de la Recherche Scientifique) and the FWO (Fonds Wetenschappelijk Onderzoek), without whom this work would not have been possible. Valentin Fortier thanks the EOS (Excellence Of Science) ET-Home project for his PhD grant. Vinciane Debaille thank the FRS-FNRS for present support. Benjamin Bultel benefitted from the support of the Research Council of Norway through its Centers of Excellence 678 funding scheme, project number 223272. Valentin Fortier would also like to thank Bernard Charlier (ULiège) for providing full access to his samples, Tiriana Segato from the 4MAT Laboratory at ULB for the XRD analyses, and finally Sabrina Cauchies for the major elements analysis of our chromite done at the Laboratoire G-Time of ULB.

References

- Adcock, C.T., Udry, A., Hauausrath, E.M., Tschauauner, O., 2018. Craters of the Moon National Monument basalts as unshocked compositional and weathering analogs for martian rocks and meteorites. *Am. Mineral.* 103, 502–516. <https://doi.org/10.2138/am-2018-6193>.
- Agee, C.B., Wilson, N.V., McCubbin, F.M., Ziegler, K., Polyak, V.J., Sharp, Z.D., Asmerom, Y., Nunn, M.H., Shaheen, R., Thiemens, M.H., Steele, A., Fogel, M.L., Bowden, R., Glamoclija, M., Zhang, Z., Elardo, S.M., 2013. Unique meteorite from early Amazonian Mars: water-rich basaltic breccia Northwest Africa 7034. *Science* 339, 780–785. <https://doi.org/10.1126/science.1228858>, 1979.
- Allen, C.C., Morris, R.V., Jager, K.M., Golden, D.C., Lindstrom, D.J., Lindstrom, MarilynM., Lockwood, J.P., 1998. Martian regolith simulant JSC Mars-1. *Lunar Planet. Sci.* XXIX, 4–5.
- Allen, D.E., Seyfried, W.E., 2003. Compositional controls on vent fluids from ultramafic-hosted hydrothermal systems at mid-ocean ridges: an experimental study at 4 00°C, 500 bars. *Geochem. Cosmochim. Acta* 67, 1531–1542. [https://doi.org/10.1016/S0016-7037\(02\)01173-0](https://doi.org/10.1016/S0016-7037(02)01173-0).
- Amador, E.S., Bandfield, J.L., Brazelton, W.J., Kelley, D., 2017. The lost city hydrothermal field. *A Spectroscopic and Astrobiological* 17, 1138–1160. <https://doi.org/10.1089/ast.2016.1606>.
- Amador, E.S., Bandfield, J.L., Thomas, N.H., 2018. A search for minerals associated with serpentinization across Mars using CRISM spectral data. *Icarus* 1–56. <https://doi.org/10.1016/j.icarus.2018.03.021>.
- Balta, J.B., Sanborn, M.E., Udry, A., Wadhwa, M., Mccsween, H.Y., 2015. Petrology and trace element geochemistry of Tissint, the newest shergottite fall. *Meteorit. Planet. Sci.* 50, 63–85. <https://doi.org/10.1111/maps.12403>.
- Barbier, S., Huang, F., Andreani, M., Tao, R., Hao, J., Eleish, A., Prabhu, A., Minhas, O., Fontaine, K., Fox, P., Daniel, I., 2020. A review of H₂, CH₄, and hydrocarbon formation in experimental serpentinization using Network analysis. *Front. Earth Sci.* 8, 1–20. <https://doi.org/10.3389/feart.2020.00209>.

- Barnes, I., O'Neil, J.R., Trescases, J.J., 1978. Present day serpentinization in New Caledonia, Oman and Yugoslavia. *Geochem. Cosmochim. Acta* 42, 144–145. [https://doi.org/10.1016/0016-7037\(78\)90225-9](https://doi.org/10.1016/0016-7037(78)90225-9).
- Basu Sarbadhikari, A., Day, J.M.D., Liu, Y., Rumble, D., Taylor, L.A., 2009. Petrogenesis of olivine-phyric shergottite Larkman Nunatak 06319: implications for enriched components in martian basalts. *Geochem. Cosmochim. Acta* 73, 2190–2214. <https://doi.org/10.1016/j.gca.2009.01.012>.
- Berndt, M.E., Allen, D.E., Seyfried, W.E., 1996. Reduction of CO₂ during serpentinization of olivine at 300 °C and 500 bar. *Geology* 24, 351–354.
- Bish, D.L., Blake, D.F., Vaniman, D.T., Chipera, S.J., Morris, R.V., Ming, D.W., Treiman, A.H., Sarrazin, P., Morrison, S.M., Downs, R.T., Achilles, C.N., Yen, A.S., Bristow, T.F., Crisp, J.A., Morookian, J.M., Farmer, J.D., Rampe, E.B., Stolper, E.M., Spanovich, N., Team, M.S., 2013. X-Ray diffraction results from Mars science laboratory: mineralogy of rocknest at Gale Crater. *Science* 1–6, 1979.
- Bost, N., Ramboz, C., LeBreton, N., Foucher, F., Lopez-Reyes, G., De Angelis, S., Josset, M., Venegas, G., Sanz-Arnan, A., Rull, F., Medina, J., Josset, J.L., Souchon, A., Ammannito, E., De Sanctis, M.C., Di Iorio, T., Carli, C., Vago, J.L., Westall, F., 2015. Testing the ability of the ExoMars 2018 payload to document geological context and potential habitability on Mars. *Planet. Space Sci.* 108, 87–97. <https://doi.org/10.1016/j.pss.2015.01.006>.
- Bost, N., Westall, F., Ramboz, C., Foucher, F., Pullan, D., Meunier, A., Petit, S., Fleischer, I., Klingelhöfer, G., Vago, J.L., 2013. Missions to Mars: characterisation of Mars analogue rocks for the international space analogue rockstore (ISAR). *Planet. Space Sci.* 113–127. <https://doi.org/10.1016/j.pss.2013.04.006>, 82–83.
- Bouvier, L.C., Costa, M.M., Connelly, J.N., Jensen, N.K., Wielandt, D., Storey, M., Nemchin, A.A., Whitehouse, M.J., Snape, J.F., Bellucci, J.J., Moynier, F., Agranier, A., Gueguen, B., Schönbräcker, M., Bizzarro, M., 2018. Evidence for extremely rapid magma ocean crystallization and crust formation on Mars. *Nature* 558, 586–589. <https://doi.org/10.1038/s41586-018-0222-z>.
- Bradley, A.S., Summons, R.E., 2010. Multiple origins of methane at the lost city hydrothermal field. *Earth Planet Sci. Lett.* 297, 34–41. <https://doi.org/10.1016/j.epsl.2010.05.034>.
- Brown, A.J., Kah, L., Mandon, L., Wiens, R., Pinet, P., Clavé, E., Mouélic, S. Le, Udry, A., Gasda, P.J., Royer, C., Hickman, K., 2023. Properties of the Nili fossae olivine-clay-carbonate lithology: orbital and in situ at séfah. Preprint.
- Bultel, B., Andréani, M., Clénet, H., Lozac, L., 2015. Deep alteration between Hellas and Isidis Basins. *Icarus* 260, 141–160. <https://doi.org/10.1016/j.icarus.2015.06.037>.
- Burghel, A., Dreibus, G., Palme, H., Rammensee, W., Spettel, B., Weckwerth, G., Wänke, H., 1983. Chemistry of Shergottites and the Shergotty parent body (SPB): further evidence for the two component model of planet formation. *Lunar Planet. Inst.* 80–81.
- Buz, J., Ehlmann, B.L., Pan, L., Grotzinger, J.P., 2017. Mineralogy and stratigraphy of the Gale crater rim, wall, and floor units. *J. Geophys. Res. Planets* 122, 1090–1118. <https://doi.org/10.1002/2016JE005163>.
- Cannon, K.M., Britt, D.T., Smith, T.M., Fritsche, R.F., Batchelder, D., 2019. Mars global simulant MGS-1: a Rocknest-based open standard for basaltic martian regolith simulants. *Icarus* 317, 470–478. <https://doi.org/10.1016/j.icarus.2018.08.019>.
- Charlier, B., Vander Auwera, J., Duchesne, J.C., 2005. Geochemistry of cumulates from the Bjerkreim-Sokndal layered intrusion (S. Norway). *Lithos* 83, 255–276. <https://doi.org/10.1016/j.lithos.2005.03.005>.
- Cloutis, E.A., Mann, P., Izawa, M.R.M., Applin, D.M., Samson, C., Kruzelecky, R., Glotch, T.D., Mertzman, S.A., Mertzman, K.R., Haltigin, T.W., Fry, C., 2015. The Canadian space agency planetary analogue materials suite. *Planet. Space Sci.* 119, 155–172. <https://doi.org/10.1016/j.pss.2015.09.001>.
- Cousin, A., Sautter, V., Fabre, C., Dromart, G., Montagnac, G., Drouet, C., Meslin, P.Y., Gasnault, O., Beyssac, O., Bernard, S., Cloutis, E., Forni, O., Beck, P., Fouchet, T., Johnson, J.R., Lasue, J., Ollila, A.M., De Parseval, P., Gouy, S., Caron, B., Madariaga, J.M., Arana, G., Madsen, M.B., Laserna, J., Moros, J., Manrique, J.A., Lopez-Reyes, G., Rull, F., Maurice, S., Wiens, R.C., 2022. SuperCam calibration targets on board the perseverance rover: fabrication and quantitative characterization. *Spectrochim. Acta Part B At. Spectrosc.* 188, 106341. <https://doi.org/10.1016/j.sab.2021.106341>.
- Crozaz, G., Floss, C., Wadhwa, M., 2003. Chemical alteration and REE mobilization in meteorites from hot and cold deserts. *Geochem. Cosmochim. Acta* 67, 4727–4741. <https://doi.org/10.1016/j.gca.2003.08.008>.
- Crozaz, G., Wadhwa, M., 2001. The terrestrial alteration of saharan shergottites dar al ganid 476 and 489: a case study of weathering in a hot desert environment. *Geochem. Cosmochim. Acta* 65, 971–977. [https://doi.org/10.1016/S0016-7037\(00\)00586-X](https://doi.org/10.1016/S0016-7037(00)00586-X).
- Dunham, E.T., Balta, J.B., Wadhwa, M., Sharp, T.G., McSween, H.Y., 2019. Petrology and geochemistry of olivine-phyric shergottites LAR 12095 and LAR 12240: implications for their petrogenetic history on Mars. *Meteorit. Planet. Sci.* 54, 811–835. <https://doi.org/10.1111/maps.13262>.
- Duyar, M.S., 2015. A Study of Catalytic Carbon Dioxide Methanation Leading to the Development of Dual Function Materials for Carbon Capture and Utilization.
- Dypvik, H., Hellevang, H., Krzesińska, A., Sætre, C., Viennet, J.C., Bultel, B., Ray, D., Poulet, F., Loizeau, D., Veneranda, M., Rull, F., Cousin, A., Werner, S.C., 2021. The Planetary Terrestrial Analogues Library (PTAL) – an exclusive lithological selection of possible martian earth analogues. *Planet. Space Sci.* 208, 105339. <https://doi.org/10.1016/j.pss.2021.105339>.
- Edwards, H.G.M., Farwell, D.W., Grady, M.M., Wynn-Williams, D.D., Wright, I.P., 1999. Comparative Raman microscopy of a Martian meteorite and Antarctic lithic analogues. *Planet. Space Sci.* 47, 353–362. [https://doi.org/10.1016/S0032-0633\(98\)00127-5](https://doi.org/10.1016/S0032-0633(98)00127-5).
- Ehlmann, B.L., Buz, J., 2014. Mineralogy and fluvial history of the watersheds of Gale, Knobel, and Sharp craters: a regional context for the Mars Science Laboratory Curiosity's exploration. *Geophys. Res. Lett.* 264–273. <https://doi.org/10.1002/2014GL02553>. Received.
- Ehlmann, B.L., Mustard, J.F., Murchie, S.L., 2010. Geologic setting of serpentine deposits. *MARS* 37, 1–5. <https://doi.org/10.1029/2010GL042596>.
- Ehlmann, B.L., Mustard, J.F., Swayze, G.A., Clark, R.N., Bishop, J.L., Poulet, F., Des Marais, D.J., Roach, L.H., Milliken, R.E., Wray, J.J., Barnouin-Jha, O., Murchie, S.L., 2009. Identification of hydrated silicate minerals on Mars using MRO-CRISM: geologic context near Nili Fossae and implications for aqueous alteration. *J. Geophys. Res. Planets* 114, 1–33. <https://doi.org/10.1029/2009JE003339>.
- Elkins-Tanton, L.T., 2008. Linked magma ocean solidification and atmospheric growth for Earth and Mars. *Earth Planet Sci. Lett.* 271, 181–191. <https://doi.org/10.1016/j.epsl.2008.03.062>.
- Elkins-Tanton, L.T., Hess, P.C., Parmentier, E.M., 2005. Possible formation of ancient crust on Mars through magma ocean processes. *J. Geophys. Res. Planets* 110, 1–11. <https://doi.org/10.1029/2005JE002480>.
- Etiopie, G., Ionescu, A., 2015. Low-temperature Catalytic CO₂ Hydrogenation with Geological Quantities of Ruthenium: a Possible Abiotic. <https://doi.org/10.1111/gfl.12106>. CH 4 source in chromitite-rich serpentinitized rocks 438–452.
- Etiopie, G., Sherwood Lollar, B., 2013. Abiotic methane on earth. *Rev. Geophys.* 51, 276–299. <https://doi.org/10.1002/rog.20011>.
- Foucher, F., Hickman-Lewis, K., Hutzler, A., Joy, K.H., Folco, L., Bridges, J.C., Wozniakiewicz, P., Martínez-Frías, J., Debaille, V., Zolensky, M., Yano, H., Bost, N., Ferrière, L., Lee, M., Michalski, J., Schroeven-Deceuninck, H., Kminek, G., Viso, M., Russell, S., Smith, C., Zipfel, J., Westall, F., 2021. Definition and use of functional analogues in planetary exploration. *Planet. Space Sci.* 197. <https://doi.org/10.1016/j.pss.2021.105162>.
- Foustoukos, D.I., Seyfried, W.E., 2004. Hydrocarbons in hydrothermal vent fluids: the role of chromium-bearing catalysts. *Science* 304, 1002–1005. <https://doi.org/10.1126/science.1096033>, 1979.
- Fries, M.D., Lee, C., Bhartia, R., Razzell Hollis, J., Beegle, L.W., Uckert, K., Graff, T.G., Abbey, W., Bailey, Z., Berger, E.L., Burton, A.S., Callaway, M.J., Cardarelli, E.L., Davis, K.N., DeFlores, L., Edgett, K.S., Fox, A.C., Garrison, D.H., Haney, N.C., Harrington, R.S., Jakubek, R.S., Kennedy, M.R., Hickman-Lewis, K., McCubbin, F.M., Miller, E., Monacelli, B., Pollock, R., Rhodes, R., Siljestrom, S., Sharma, S., Smith, C. L., Steele, A., Sylvia, M., Tran, V.D., Weiner, R.H., Yanchilina, A.G., Aileen Yingst, R., 2022. The SHERLOC calibration target on the Mars 2020 perseverance rover: design, operations, outreach, and future human exploration functions. *Space Sci. Rev.* 218, 1–33. <https://doi.org/10.1007/s11214-022-00907-1>.
- Gleason, J.D., Kring, D.A., Hill, D.H., Boynton, W.V., 1997. Petrography and bulk chemistry of Martian Iherzolite LEW88516. *Geochem. Cosmochim. Acta* 61, 4007–4014. [https://doi.org/10.1016/S0016-7037\(97\)00196-8](https://doi.org/10.1016/S0016-7037(97)00196-8).
- Greshake, A., Fritz, J., Stöffler, D., 2004. Petrology and shock metamorphism of the olivine-phyric shergottite Yamato 980459: evidence for a two-stage cooling and a single-stage ejection history. *Geochem. Cosmochim. Acta* 68, 2359–2377. <https://doi.org/10.1016/j.gca.2003.11.022>.
- Hamilton, V.E., Christensen, P.R., McSween, H.Y., Bandfield, J.L., 2003. Searching for the source regions of martian meteorites using MGS TES: integrating martian meteorites into the global distribution of igneous materials. *MARS* 885, 871–885.
- Harvey, R.P., Wadhwa, M., McSween, H.Y., Crozaz, G., 1993. Petrography, mineral chemistry, and petrogenesis of Antarctic Shergottite LEW88516. *Geochem. Cosmochim. Acta* 57, 4769–4783. [https://doi.org/10.1016/0016-7037\(93\)90199-7](https://doi.org/10.1016/0016-7037(93)90199-7).
- Hickman-Lewis, K., Foucher, F., Pelletier, S., Messori, F., Westall, F., 2020. Geological appraisals of core samples using the ExoMars 2020 rover instrumentation. *Planet. Space Sci.* 180. <https://doi.org/10.1016/j.pss.2019.104743>.
- Horita, J., Berndt, M.E., 1999. Abiogenic methane formation and isotopic fractionation under hydrothermal conditions. *Science* 285, 1055–1058.
- Hsu, W., Guan, Y., Wang, H., Leshin, L.A., Wang, R., Zhang, W., Chen, X., Zhang, F., Lin, C., 2004. The Iherzolitic shergottite Grove Mountains 99027: rare earth element geochemistry. *Meteorit. Planet. Sci.* 39, 701–709. <https://doi.org/10.1111/j.1945-5100.2004.tb00113.x>.
- Humayun, M., Nemchin, A., Zanda, B., Hewins, R.H., Grange, M., Kennedy, A., Lorand, J. P., Göpel, C., Fieni, C., Pont, S., Deldicque, D., 2013. Origin and age of the earliest Martian crust from meteorite NWA 7533. *Nature* 503, 513–516. <https://doi.org/10.1038/nature12764>.
- Jiang, Y., Hsu, W., 2012. Petrogenesis of Grove Mountains 020090: an enriched “Iherzolitic” shergottite. *Meteorit. Planet. Sci.* 47, 1419–1435. <https://doi.org/10.1111/j.1945-5100.2012.01404.x>.
- Karl, D., Cannon, K.M., Gurlo, A., 2022. Review of space resources processing for Mars missions: martian simulants, regolith bonding concepts and additive manufacturing. *Open Ceramics* 9, 100216. <https://doi.org/10.1016/j.oceram.2021.100216>.
- Lapen, T.J., Righter, M., Andreasen, R., Irving, A.J., Satkoski, A.M., Beard, B.L., Nishiizumi, K., Jull, A.J.T., Caffee, M.W., 2017. Two billion years of magmatism recorded from a single Mars meteorite ejection site. *Sci. Adv.* 3, 1–7. <https://doi.org/10.1126/sciadv.1600922>.
- Leeman, W.P., Vitaliano, C.J., 1976. Petrology of McKinney basalt, snake river plain, Idaho. *Bull. Geol. Soc. Am.* 87, 1777–1792. [https://doi.org/10.1130/0016-7606\(1976\)87<1777:POMBSR>2.0.CO;2](https://doi.org/10.1130/0016-7606(1976)87<1777:POMBSR>2.0.CO;2).
- Lin, Y., Guan, Y., Wang, D., Kimura, M., Leshin, L.A., 2005. Petrogenesis of the new Iherzolitic shergottite Grove Mountains 99027: constraints of petrography, mineral chemistry, and rare earth elements. *Meteorit. Planet. Sci.* 40, 1599–1619. <https://doi.org/10.1111/j.1945-5100.2005.tb00134.x>.
- Lodders, K., 1998. A survey of shergottite, nakhlite and chassigny meteorites whole-rock compositions. *Meteorites Planet. Sci.* 83, 183–190.
- Maeda, R., Goderis, S., Debaille, V., Pourkhorsandi, H., Hublet, G., Claeys, P., 2021. The effects of Antarctic alteration and sample heterogeneity on Sm-Nd and Lu-Hf

- systematics in H chondrites. *Geochem. Cosmochim. Acta* 305, 106–129. <https://doi.org/10.1016/j.gca.2021.05.005>.
- Ma, M., Laul, J.C., Schmitt, R.A., 1981. Analogous and Complementary Rare Earth Element Patterns on Meteorite Parent Bodies and the Earth Inferred from a Study of the Achondrite ALH 77005, Other Unique Achondrites and the Shergottites. *Lunar and Planetary Institute*.
- Mandon, L., Parkes Bowen, A., Quantin-Nataf, C., Bridges, J.C., Carter, J., Pan, L., Beck, P., Dehouck, E., Volat, M., Thomas, N., Cremonese, G., Tornabene, L.L., Thollet, P., 2021. Morphological and spectral diversity of the clay-bearing unit at the ExoMars landing site Oxia Planum. *Astrobiology* 21, 464–480. <https://doi.org/10.1089/ast.2020.2292>.
- Manzari, P., De Angelis, S., De Sanctis, M.C., Di Iorio, T., Ammannito, E., Bost, N., Foucher, F., Westall, F., 2016. Microimaging VIS-IR spectroscopy of ancient volcanic rocks as Mars analogues. *Earth Space Sci.* 268–281. <https://doi.org/10.1002/2015EA000153>. Received.
- Martin, B., Fyfe, W.S., 1970. Some experimental and theoretical observations on the kinetics of hydration reactions with particular reference to serpentinization. *Chem. Geol.* [https://doi.org/10.1016/0009-2541\(70\)90018-5](https://doi.org/10.1016/0009-2541(70)90018-5).
- McCullom, T.M., 2016. Abiotic Methane Formation during Experimental Serpentinization of Olivine. <https://doi.org/10.1073/pnas.1611843113>.
- McCullom, T.M., Klein, F., Moskowitz, B., Solheid, P., 2022. Experimental serpentinization of iron-rich olivine (hortonolite): implications for hydrogen generation and secondary mineralization on Mars and icy moons. *Geochem. Cosmochim. Acta* 335, 98–110. <https://doi.org/10.1016/j.gca.2022.08.025>.
- McCullom, T.M., Seewald, J.S., 2013. Serpentinities, hydrogen, and life. *Elements* 9, 129–134. <https://doi.org/10.2113/gselements.9.2.129>.
- McCullom, T.M., Seewald, J.S., 2007. Abiotic synthesis of organic compounds in deep-sea hydrothermal environments. *Chem. Rev.* 107, 382–401. <https://doi.org/10.1021/cr0503660>.
- McSween, H.Y., 2015. Petrology on Mars. *Am. Mineral.* 100, 2380–2395. <https://doi.org/10.2138/am-2015-5257>.
- McSween, H.Y., Jarosewich, E., 1983. Petrogenesis of the Elephant Moraine A79001 meteorite: multiple magma pulses on the shergottite parent body. *Geochem. Cosmochim. Acta* 47, 1501–1513. [https://doi.org/10.1016/0016-7037\(83\)90309-5](https://doi.org/10.1016/0016-7037(83)90309-5).
- McSween, H.Y., Jeffrey Taylor, G., Wyatt, M.B., 2009. Elemental composition of the martian crust. *Science* 324, 736–739. <https://doi.org/10.1126/science.1165871>, 1979.
- Ménez, B., 2020. Abiotic hydrogen and methane: fuels for life. *Elements* 16, 39–46. <https://doi.org/10.2138/GSELEMENTS.16.1.39>.
- Michalski, J.R., Niles, P.B., 2010. Deep crustal carbonate rocks exposed by meteor impact on Mars. *Nat. Geosci.* 3, 751–755. <https://doi.org/10.1038/ngeo971>.
- Miguel, C.V., Soria, M.A., Mendes, A., Madeira, L.M., 2015. Direct CO₂ hydrogenation to methane or methanol from post-combustion exhaust streams - a thermodynamic study. *J. Nat. Gas Sci. Eng.* 22, 1–8. <https://doi.org/10.1016/j.jngse.2014.11.010>.
- Mikouchi, T., Kurihara, T., 2008. Mineralogy and petrology of paired lherzolitic shergottites Yamato 000027, Yamato 000047, and Yamato 000097: another fragment from a Martian “lherzolite” block. *Pol. Sci.* 2, 175–194. <https://doi.org/10.1016/j.polar.2008.06.003>.
- Mikouchi, T., Miyamoto, M., 1997. Yamato-793605: a new lherzolitic shergottite from the Japanese antarctic meteorite collection. *Antarct. Meteor. Res.* 10.
- Muirhead, B.K., Nichol, A.K., Umland, J., Sutherland, O., Vijendran, S., 2020. Mars sample return campaign concept status. *Acta Astronaut.* 176, 131–138. <https://doi.org/10.1016/j.actaastro.2020.06.026>.
- Müller, W.F., 1993. Thermal and deformation history of the Shergotty meteorite deduced from clinopyroxene microstructure. *Geochem. Cosmochim. Acta* 57, 4311–4322. [https://doi.org/10.1016/0016-7037\(93\)90325-Q](https://doi.org/10.1016/0016-7037(93)90325-Q).
- Mustard, J.F., Ehlmann, B.L., Murchie, S.L., Poulet, F., Mangold, N., Head, J.W., Bibring, J.P., Roach, L.H., 2009. Composition, morphology, and stratigraphy of Noachian crust around the Isidis basin. *J. Geophys. Res. Planets* 114, 1–18. <https://doi.org/10.1029/2009JE003349>.
- Mustard, J.F., Poulet, F., Head, J.W., Mangold, N., Bibring, J.P., Pelkey, S.M., Fassett, C. I., Langevin, Y., Neukum, G., 2007. Mineralogy of the Nili fossae region with OMEGA/Mars express data: 1. Ancient impact melt in the isidis basin and implications for the transition from the Noachian to hesperian. *J. Geophys. Res. Planets* 112, 1–14. <https://doi.org/10.1029/2006JE002834>.
- Namur, O., Charlier, B., Toplis, M.J., Higgins, M.D., Liégeois, J.P., vander Auwera, J., 2010. Crystallization sequence and magma chamber processes in the ferrobaltic Sept Iles layered intrusion, Canada. *J. Petrol.* 51, 1203–1236. <https://doi.org/10.1093/petrology/egq016>.
- Nyquist, L.E., Bogard, D.D., Shih, C.-Y., Greshake, A., Stöffler, D., Eugster, O., 2001. Ages and Geologic Histories of Martian Meteorites 105–164. https://doi.org/10.1007/978-94-017-1035-0_5.
- Okland, I., Huang, S., Thorseth, I.H., Pedersen, R.B., 2014. Formation of H₂, CH₄ and N₂ species during low-temperature experimental alteration of ultramafic rocks. *Chem. Geol.* 387, 22–34. <https://doi.org/10.1016/j.chemgeo.2014.08.003>.
- Oze, C., Sharma, M., 2005. Have olivine, will gas: serpentinization and the abiogenic production of methane on Mars. *Geophys. Res. Lett.* 32, 10–13. <https://doi.org/10.1029/2005GL022691>.
- Papike, J.J., Karner, J.M., Shearer, C.K., Burger, P.V., 2009. Silicate mineralogy of martian meteorites. *Geochem. Cosmochim. Acta* 73, 7443–7485. <https://doi.org/10.1016/j.gca.2009.09.008>.
- Peters, G.H., Abbey, W., Bearman, G.H., Mungas, G.S., Smith, J.A., Anderson, R.C., Douglas, S., Beegle, L.W., 2008. Mojave Mars simulant-Characterization of a new geologic Mars analog. *Icarus* 197, 470–479. <https://doi.org/10.1016/j.icarus.2008.05.004>.
- Pourkhorsandi, H., Debaille, V., Armitage, R.M., Van Ginneken, M., Rochette, P., Gattacceca, J., 2021. The effects of terrestrial weathering on samarium neodymium isotopic composition of ordinary chondrites. *Chem. Geol.* 562 <https://doi.org/10.1016/j.chemgeo.2020.120056>.
- Quantin-Nataf, C., Carter, J., Mandon, L., Thollet, P., Balme, M., Volat, M., Pan, L., Loizeau, D., Millot, C., Breton, S., Dehouck, E., Fawdon, P., Gupta, S., Davis, J., Grindrod, P.M., Pacifici, A., Bultel, B., Allemand, P., Ody, A., Lozach, L., Broyer, J., 2021. Oxia Planum: the landing site for the ExoMars “rosalind franklin” rover mission: geological context and prelanding interpretation. *Astrobiology* 21, 345–366. <https://doi.org/10.1089/ast.2019.2191>.
- Ramkisson, N.K., Pearson, V.K., Schwenzer, S.P., Schröder, C., Kimbauer, T., Wood, D., Seidel, R.G.W., Miller, M.A., Olsson-Francis, K., 2019. New simulants for martian regolith: controlling iron variability. *Planet. Space Sci.* 179 <https://doi.org/10.1016/j.pss.2019.104722>.
- Sautter, V., Toplis, M.J., Wiens, R.C., Cousin, A., Fabre, C., Gasnault, O., Maurice, S., Forni, O., Lasue, J., Ollila, A., Bridges, J.C., Mangold, N., Le Mouélic, S., Fisk, M., Meslin, P.Y., Beck, P., Pinet, P., Le Deit, L., Rapin, W., Stolper, E.M., Newsom, H., Dyar, D., Lanza, N., Vaniman, D., Clegg, S., Wray, J.J., 2015. In situ evidence for continental crust on early Mars. *Nat. Geosci.* 8, 605–609. <https://doi.org/10.1038/ngeo2474>.
- Schrenk, M.O., Brazelton, W.J., Lang, S.Q., 2013. Serpentinization, carbon, and deep life. *Rev. Mineral. Geochem.* 75, 575–606. <https://doi.org/10.2138/rmg.2013.75.18>.
- Steele, I.M., Smith, J.V., 1982. Petrography and mineralogy of two basalts and olivine-pyroxene-spinel fragments in achondrite EETA79001. *J. Geophys. Res.* 87 <https://doi.org/10.1029/jb087is01p0a375>.
- Stöffler, D., Ostertag, R., Jammes, C., Pfannschmidt, G., Gupta, P.R.S., Simon, S.B., Papike, J.J., Beauchamp, R.H., 1986. Shock metamorphism and petrography of the Shergotty achondrite. *Geochem. Cosmochim. Acta* 50, 889–903. [https://doi.org/10.1016/0016-7037\(86\)90371-6](https://doi.org/10.1016/0016-7037(86)90371-6).
- Treiman, A.H., 2005. The nakhlite meteorites: augite-rich igneous rocks from Mars. *Chem. Erde* 65, 203–270. <https://doi.org/10.1016/j.chemer.2005.01.004>.
- Treiman, A.H., 1994. Comparison of the LEW88516 and ALHA77005 martian meteorites: similar but distinct. *Meteoritics* 29, 581–592. <https://doi.org/10.1111/j.1945-5100.1994.tb00771.x>.
- Udry, A., Day, J.M.D., 2018. 1.34 billion-year-old magmatism on Mars evaluated from the co-genetic nakhlite and chassignite meteorites. *Geochem. Cosmochim. Acta* 238, 292–315. <https://doi.org/10.1016/j.gca.2018.07.006>.
- Udry, A., Howarth, G.H., Herd, C.D.K., Day, J.M.D., Lapen, T.J., Filiberto, J., 2020. What martian meteorites reveal about the interior and surface of Mars. *J. Geophys. Res. Planets* 125, 1–34. <https://doi.org/10.1029/2020JE006523>.
- Usui, T., Sanborn, M., Wadhwa, M., McSween, H.Y., 2010. Petrology and trace element geochemistry of Robert Massif 04261 and 04262 meteorites, the first examples of geochemically enriched lherzolitic shergottites. *Geochem. Cosmochim. Acta* 74, 7283–7306. <https://doi.org/10.1016/j.gca.2010.09.010>.
- Viviano-Beck, C.E., Murchie, S.L., Beck, A.W., Dohm, J.M., 2017. Compositional and structural constraints on the geologic history of eastern Tharsis Rise, Mars. *Icarus* 284, 43–58. <https://doi.org/10.1016/j.icarus.2016.09.005>.
- Webster, C.R., Mahaffy, P.R., Atreya, S.K., Flesch, G.J., Mischna, M.A., Meslin, P.Y., Farley, K.A., Conrad, P.G., Christensen, L.E., Pavlov, A.A., Martín-Torres, J., Zorzano, M.P., McConnochie, T.H., Owen, T., Eigenbrode, J.L., Glavin, D.P., Steele, A., Malespin, C.A., Archer, P.D., Sutter, B., Coll, P., Freissinet, C., McKay, C.P., Moores, J.E., Schwenzer, S.P., Bridges, J.C., Navarro-Gonzalez, R., Gellert, R., Lemmon, M.T., 2015. Mars methane detection and variability at Gale crater. *Science* 347, 415–417. <https://doi.org/10.1126/science.1261713>, 1979.
- Wentworth, S.J., Gibson, E.K., Velbel, M.A., McKay, D.S., 2005. Antarctic dry valleys and indigenous weathering in Mars meteorites: implications for water and life on Mars. *Icarus* 174, 383–395. <https://doi.org/10.1016/j.icarus.2004.08.026>.
- Wieczorek, M.A., Broquet, A., McLennan, S.M., Rivoldini, A., Golombek, M., Antonangeli, D., Beghein, C., Giardini, D., Gudkova, T., Gyalay, S., Johnson, C.L., Joshi, R., Kim, D., King, S.D., Knapmeyer-Endrun, B., Lognonné, P., Michaut, C., Mittelholz, A., Nimmo, F., Ojha, L., Panning, M.P., Plesa, A.C., Siegler, M.A., Smrekar, S.E., Spohn, T., Banerdt, W.B., 2022. InSight constraints on the global character of the martian crust. *J. Geophys. Res. Planets* 127, 1–35. <https://doi.org/10.1029/2022JE007298>.
- Wieler, R., Huber, L., Busemann, H., Seiler, S., Leya, I., Maden, C., Masarik, J., Nw, C., 2016. Noble Gases in 18 Martian Meteorites and Angrite Northwest Africa 7812 — Exposure Ages, Trapped Gases, and a Re-evaluation of the Evidence for Solar Cosmic Ray-Produced Neon in Shergottites and Other Achondrites, 428, pp. 407–428. <https://doi.org/10.1111/maps.12600>.
- Wiens, R.C., Udry, A., Beyssac, O., Quantin-Nataf, C., Mangold, N., Cousin, A., Mandon, L., Bosak, T., Forni, O., McLennan, S.M., Sautter, V., Brown, A., Benzerara, K., Johnson, J.R., Mayhew, L., Maurice, S., Anderson, R.B., Clegg, S.M., Crumpler, G., Gabriel, T.S.J., Gasda, P., Hall, J., Horgan, B.H.N., Kah, L., Legett IV, C., Madariaga, J.M., Meslin, P.Y., Ollila, A.M., Poulet, F., Royer, C., Sharma, S.K., Siljeström, S., Simon, J.L., Acosta-Maeda, T.E., Alvarez-Llamas, C., Angel, S.M., Arana, G., Beck, P., Bernard, S., Bertrand, T., Bousquet, B., Castro, K., Chide, B., Clavé, E., Cloutis, E., Connell, S., Dehouck, E., Dromart, G., Fischer, W., Fouchet, T., Francis, R., Frydenvang, J., Gasnault, O., Gibbons, E., Gupta, S., Hausrath, E.M., Jacob, X., Kalucha, H., Kelly, E., Knutsen, E., Lanza, N., Laserna, J., Lasue, J., Le Mouélic, S., Leveille, R., Reyes, G.L., Lorenz, R., Manrique, J.A., Martínez-Frías, J., McConnochie, T., Melikechi, N., Mimoun, D., Montmessin, F., Moros, J., Murdoch, N., Pilleri, P., Pilorget, C., Pinet, P., Rapin, W., Rull, F., Schröder, S., Shuster, D.L., Smith, R.J., Stott, A.E., Tarnas, J., Turenne, N., Veneranda, M., Vogt, D.S., Weiss, B.P., Willis, P., Stack, K.M., Williford, K.H., Farley, K.A., 2022. Compositionally and density stratified igneous terrain in Jezero crater, Mars. *Sci. Adv.* 8 <https://doi.org/10.1126/sciadv.abo3399>.